RSC Advances

PAPER

View Article Online
View Journal | View Issue

Cite this: *RSC Adv.*, 2022, **12**, 31338

Hydrogen peroxide modified and bismuth vanadate decorated titanium dioxide nanocomposite ($BiVO_4$@HMT) for enhanced visible light photocatalytic growth inhibition of harmful cyanobacteria in water†

Jamshaid Rashid, ‡*[ab] Fatima Imtiaz,‡[b] Ming Xu[a] and Irina N. Savina[c]

The persistence of harmful cyanobacterial algal blooms in aquatic ecosystems leads to health damage for various life forms. In this study, a photocatalyst active in the visible light range was prepared by combining $BiVO_4$ with hydrogen peroxide modified titanium dioxide ($BiVO_4$@HMT; for short), using an impregnation method. The catalyst was used to photocatalytically inhibit the growth of cyanobacteria collected from a bloom site. To infer the optimum pH for cyanobacterial growth, the effect of pH was studied. The growth of cyanobacteria was favoured in an alkaline environment at pH values in the range of 8–9.5 when analysed on the 20th day of incubation. Structural and chemical analysis of pristine and composite nano-powders was performed using XRD, SEM, TEM and XPS, confirming the heterojunction formation, while optical and band gap analysis revealed increased visible light absorption and reduced band gap of the composite. A small strawberry seed-like assembly of $BiVO_4$ particles increased the light absorption in the 15%$BiVO_4$@HMT composite and increased the inhibition efficiency up to 2.56 times compared to pristine HMT at an exposure time of 6 h and cell concentration at 0.1 g L^{-1} with an optimum catalyst dose of 1 g L^{-1}. The amount of chlorophyll *'a'* decreased due to the generation of catalytically reactive species, especially holes (h^+), which caused oxidative damage to the cell wall, cell membrane and antioxidants in algal cells. This study reports that visible light active nanocatalysts can be used as a promising method for reducing algal blooms in water bodies.

Received 24th August 2022
Accepted 25th October 2022

DOI: 10.1039/d2ra05317a

rsc.li/rsc-advances

1. Introduction

Cyanobacteria, also known as blue-green algae, are photoautotrophic Gram-negative bacteria, the main component of phytoplankton in fresh, marine, and brackish waters. Cyanobacteria can grow uncontrollably due to prevalence of growth-suitable conditions such as additional nutrient content, light availability, increased temperature and pH, and variation in climate scenarios, thus triggering cultural eutrophication,[1–3] presenting the appearance of thick foam-like 'pea-soup' on the surface of the water, associated with decreased water transparency, increased pH, and hence deteriorated water quality. Cyanobacteria release taste and smell compounds such as geosmin and methyl-isoborneol (MIB), sources of nuisance.[4,5] Various cyanobacterial species, *Microcystis*, *Anabaena*, *Aphanothece* and others, release toxic compounds known as microcystins or cyanotoxins (MC-LR, -RR,-YR) in water bodies, which cause hepatic and dermal cancer, digestive and neurological disorders, so, can pose deleterious effects on humans and aquatic life forms.[6,7]

It's a huge challenge to stop, prevent and mitigate the global expansion of harmful cyanobacterial algal blooms (Cyano-HABs). So far, many strategies have been developed to control their growth, which include sonication,[8] physical control tactics,[9,10] chemical mitigation strategies,[11] biological control methods,[12] and others. All these approaches have the potential to control algal growth, but in practice they are too difficult to achieve effective results in natural aquatic systems.[13,14] Chemicals either in pure or chelated forms has disadvantages associated with environmental persistence and toxicity to non-target organisms,[15] moreover, reinvasion of cyanobacterial cells occur after the toxic effects of the chemical have disappeared.[16] Urrutia and co-workers[17] found that 'aquatic bio-manipulation' can be used to control cyanobacterial biomass, but biological

[a]*BNU-HKUST Laboratory for Green Innovation, Advanced Institute of Natural Sciences, Beijing Normal University at Zhuhai, Zhuhai 519087, China. E-mail: jamshaidrashid@gmail.com*

[b]*Department of Environmental Science, Faculty of Biological Sciences, Quaid-I-Azam University, Islamabad 45320, Pakistan*

[c]*School of Applied Sciences, University of Brighton, Huxley Building, Lewes Road, Brighton BN2 4GJ, UK*

† Electronic supplementary information (ESI) available. See DOI: https://doi.org/10.1039/d2ra05317a

‡ Authors contributed equally to this work.

control takes longer to work in natural water bodies, and the periodic bio-manipulation can be dangerous to the food web and biodiversity.[18]

Among many advanced oxidation processes (AOPs), photocatalysis has proven to be powerful in the modern era to mitigate the growth of cyanobacteria and their toxins, as well as other water pollutants, without leaving any by-products.[19,20] Photocatalysis is a light-mediated process that leads to the formation of reactive oxidation species (ROSs) which can irreversibly damage cellular matters, including the protein structure of chlorophyll complex, secondary metabolites, and odoriferous compounds.[21,22] In recent years, several studies have been focused on the ability of TiO_2, the first photocatalytic semiconductor, to kill various bacteria and cyanobacteria. Owing to its wider band gap of 3.0–3.2 eV, activity occurs only under the exposure of ultraviolet (UV) light (320 nm < λ < 400 nm), which limits the use of TiO_2 for bloom removal.[23] Therefore, it is extremely important to study various methods of narrowing its band structure for absorption of light in the visible range (λ > 400 nm). The modification of TiO_2 (Degussa P25) with the addition of hydrogen peroxide (H_2O_2) has proven effective in removing of organic water pollutants by responding the sun light.[24,25] Basically, H_2O_2 and TiO_2 by themselves cannot absorb light in the visible region, but when they combine, the –OOH group of H_2O_2 replaces its –OH group at the surface of titania particles resulting in the formation of titanium peroxide, forming peroxo-complexes expressing yellowish colour. The complexes formed, shift the absorption spectrum of titania from the UV to the visible region.[26] To the best of our knowledge, there have been no studies involving the use of TiO_2 modified with hydrogen peroxide (HMT) to inhibit the growth of cyanobacteria. Furthermore, among Bi-based semiconductors[27,28] bismuth vanadate ($BiVO_4$) has gained importance since the last decade due to its remarkable properties, as a non-toxic photocatalyst with excellent chemical, electrical and photonic characteristics. Among three crystalline forms 'monoclinic scheelite' is the most active as a photocatalyst due to its lower band gap of 2.4 eV.[29] It was reported that the narrow band gap of $BiVO_4$ is achieved due to the hybridized O 2p and 6s orbital in the valence band of Bi which helps the 'photoexcited electron' travel a short distance to the 3d orbital of vanadium.[30] The literature has reported rare attempts to disinfect water from *E. coli*[31] and cyanotoxins[32] using $BiVO_4$ as an active photocatalyst.

Therefore, current study reports the synthesis of H_2O_2 modified TiO_2 (HMT) and $BiVO_4$, as well as the construction of $BiVO_4$@HMT composites and their use to inhibit the growth of locally isolated cyanobacteria. For this purpose cells were used in experimental suspension after harvesting the biomass instead of their counting, thus, excluding the laborious step and excessive instrumentation. To best of our information, the H_2O_2 modified TiO_2 (HMT) and $BiVO_4$@HMT have not been reported for anti-algal applications.

2. Materials and methods

2.1. Reagents and chemicals

Bismuth nitrate ($Bi(NO_3)_3 \cdot 5H_2O$), ammonium vanadate (NH_4VO_3), titanium dioxide (Degussa P25), hydrogen peroxide (H_2O_2), nitric acid (HNO_3) were purchased from Sigma Aldrich (USA), ammonium hydroxide (NH_4OH), ethanol, acetone and BG-11 ingredients were purchased from VWR International (USA). All chemicals were of analytical grade and used without purification.

2.2. Cyanobacterial cell culture and growth medium

The cyanobacterial cells used in this study were locally isolated from a eutrophicated site in Islamabad. A sample was collected from the sewage treatment plan \ (Islamabad, Pakistan). The isolated culture was cultivated in BG-11 medium prepared and autoclaved according to the method provided by Fraunhofer CCCryo (Culture Collection of Cryophilic Algae) laboratories (ESI 1.1†). The algal culture was cultivated in Erlenmeyer flasks placed in an in-house fabricated wooden chamber at 25 °C ± 2 °C, at intensity of 1000 Lux having 12/12 h light: dark cycles. Growth flasks were agitated three times a day to avoid any cellular deposition and self-shading effect.

2.2.1. Effect of pH on cyanobacterial growth. To test the effect of pH on cyanobacterial growth, suitable amount of prepared BG-11 media was added to test tubes after adjusting the pH to a range of 2–12 with 4 M NH_4OH and 4 M HNO_3, followed by sterilization. After cooling, each experiment and control tube was inoculated with 1 mL of cell culture going through its stationary phase, while the pH for control systems was kept to be 8.05. All tubes were placed in a growth chamber provided with cool white lights for 12 : 12 light and dark cycles at 1000 Lux and 25 °C ± 2 °C. Incubation experiments were performed in duplicate, and the growth of cyanobacteria was analysed by measuring the increase in chlorophyll '*a*' concentration using UV-Vis spectrophotometer 20 days after incubation.

2.3. Synthesis of $BiVO_4$, HMT and $BiVO_4$@HMT

$BiVO_4$ nanoparticles were synthesized by the sol–gel method according to the method described by Pookmanee.[33] Stoichiometric amounts (0.003 M) of $Bi(NO_3)_3 \cdot 5H_2O$ and NH_4VO_3 were dissolved in 5 mL of 4 M HNO_3 and 4 M NH_4OH, respectively. After stirring individually for 30 min, both solutions were mixed together to generate a yellow solution. To the resulting solution 10 mL of absolute ethanol was added, and the temperature was maintained at 70 °C with continuous stirring for 1 h. The sol turned into a yellow gel upon addition of 5 mL of deionized water and 0.5 mL of 1 M acetic acid. The resulting gel was dried in an oven at 100 °C, ground using pestle and mortar and calcined in Muffle Furnace (Ney® VULCAN) at 600 °C for 2 h (Fig. S1(a)†).

Modified titanium powders (HMT), were produced by soaking and heat-drying method,[24] briefly, 1.5 g of TiO_2 (Degussa P25) was soaked in 30 mL of 3% H_2O_2. The obtained suspension was stirred for 1 h, filtered and dried at 60 °C for 3 h. The dried yellowish material was mechanically ground to a fine powder using a pestle and mortar (Fig. S1(b)†).

$BiVO_4$/HMT composites with variable percent content of $BiVO_4$ (5–20%) were constructed *via* impregnation method, using HMT as the base material. During the composite

production, the stoichiometric amounts of $BiVO_4$ precursors were used to obtain 5%, 10%, 15% and 20% of $BiVO_4$, respectively. The solutions were stirred for 30 min individually, followed by the addition of the calculated amount of HMT in each solution mixture; further process was identical to fabrication of $BiVO_4$ as mentioned earlier.

2.3.1. Analytical methods. The crystalline nature of the synthesized nano-powders was characterized by X-ray diffraction (XRD, Bruker AXS- D8, Germany) using Cu-Kα ($\lambda = 1.5406$ nm) as a radiation source and a secondary monochromator in the 2θ range from 10 to 80°. The surface morphologies of the samples were investigated using Scanning Electron Microscopy (SEM) (Hitachi S-4800) at an operating voltage of 25 kV. To confirm the chemical and elemental composition of the materials, Energy Dispersive X-ray Spectroscopy (EDAX) analysis was performed using the Omicron system (Al Kα 1486.7 eV X-ray source operated at 15 KeV). To obtain images of the internal structures of materials, Transmission Electron Microscopy (TEM) were implemented on a JEOL (JEM-2100) electron microscope operating at the voltage of 20 kV. The band gap was confirmed by the plot of $(\alpha h\nu)^{1/2}$ *versus* $h\nu$; determined by the Tauc's relation, which is written as $\alpha h\nu = A(h\nu - E_g)^n$; where h is the Plank's constant, ν is the frequency of photons, α represents the absorption coefficient, A is constant, E_g is band gap and $n = 1/2$ is a constant that depends on the semiconductor's transition type.[34,35]

2.4. Photocatalytic growth inhibition of cyanobacteria

2.4.1. Algal harvesting and cell suspension. The cultivated cell culture was harvested during the stationary growth phase; on about 35th day, using a Jouan centrifuge S/N 3021912 having AB 2.14 10 000*g* swing rotor, where the cells were centrifuged at 3500 RPM. The harvested algae in the form of pellets were stored at 2–4 °C. For photocatalytic experiments, cell suspensions from the harvested algae at 0.1 g L^{-1} (dry weight equivalent) were prepared, maintaining a solution volume of 120 mL. The catalyst was added in the desired dose and exposed to visible light in a photo-reactor for 6 h, and 10 mL aliquots of samples were collected at 0 to 6 h.

2.4.2. Photocatalytic experiments. Preliminary experiments were performed to test the inhibition of cyanobacterial growth by exposing cells (0.1 g L^{-1}) to synthesized nanomaterials at different doses under visible light irradiation at pH 6.9. All experiments were conducted in duplicates. To evaluate the effect of the solution pH on the catalyst and cell, 3 pH values (5, 7 and 9) were selected by using 0.5 M acidic and basic solutions to adjust the pH. For all photocatalytic activities under visible light, a Luzchem photochemical reactor (LZC-4V) was used for studies with irradiation of (14 × 8 W each) Slovenia cool white lamps (λ = 390–700 nm) and a spectral irradiance of 17.45 mW cm^{-2}, monitored by a Luzchem power monitor at 12 cm from the light source.

2.4.3. Chlorophyll '*a*' analysis for growth inhibition. Cyanobacterial growth inhibition was indicated by measuring the chlorophyll '*a*' content, estimated in accordance with the bio-protocol[36] for measuring chlorophyll content (ESI 1.2.†). The percentage growth inhibition was estimated using the following formula:

$$\text{Cyanobacterial inhibition efficiency (\%)} = (C_0 - C_t/C_0) \times 100 \quad (1)$$

where, C_0 refers to the absorbance of control group and C_t corresponds to absorbance at specific time interval.[37]

3. Results and discussion

3.1. Morphology and microstructural characterizations

$BiVO_4$, HMT and $BiVO_4$@HMT were synthesized as described in the methods. $BiVO_4$@HMT composites with 5%, 10%, 15% and 20% of $BiVO_4$ were prepared to analyse the effect of $BiVO_4$ inclusion on catalytic activity. The SEM images of HMT (Fig. 1a–c) show that the particles have nanometer dimensions with the size range from 30 to 75 nm and irregular shape. Agglomeration of the synthesized $BiVO_4$ particles was evident in Fig. 1d–f, which means that the size and shape of crystal depends on calcination temperature,[38] as at high calcination temperature, the lattice parameters of same crystal system tend to decrease followed by change in the size and shape of the crystallite[39,40] while these prepared particles have an irregular disc shape with a particle diameter < 300 nm (Fig. 1e).

The TEM analysis shows the smaller size of HMT particles (Fig. 2a and b), less than 50 and 100 nm in diameter and the shape of the particles varies from spherical to rectangle. Fig. 2c and d shows a 10%$BiVO_4$/HMT composite where the surface of HMT seems to be decorated with larger lamellar particles of $BiVO_4$, which have small strawberry seeds like appearances on the surface. Fig. 2e and f shows the 15%$BiVO_4$/HMT with a denser lamellar appearance inside the modified titania nanoparticles. This close contact between the two nanocatalysts created a heterojunction that would increase charge carriers separation. The results are in good agreement with the crystalline consistency shown on XRD (Fig. 3).

3.2. X-ray diffraction

The crystallinity and phases of pristine HMT, $BiVO_4$ and their nanocomposite 15%$BiVO_4$@HMT were analysed using X-ray diffraction (Fig. 3). The diffraction peaks of H_2O_2 modified (HM) Degussa-P25 are in good agreement with the results reported by Kang and co-workers[41,42] and correspond to JCDPS card numbers 88–1175 for anatase (A) and 84–1286 for rutile (R) phase.[43,44] The diffraction peaks of the prepared samples were the same as those of pure P25, which indicates the purity of the sample and the fact that the modification with H_2O_2 didn't cause any changes in the crystal structure. The modification with H_2O_2 and microwave drying has increased the intensities of XRD peaks indicating improved crystallinity. The diffraction peaks of $BiVO_4$ were indorsed to the monoclinic $BiVO_4$ JCDPS card file no. 14-0688.[45] The more intense peaks appeared at 2θ = 18.8° and 28.9° correspond to hkl values of (011) and (121) at 600 °C, which may be attributed to a decrease in the full width at half maximum (FWHM) representing temperature dependence of crystal size.[38] The lattice parameters for the diffraction peaks were $a = 5.195$ Å, $b = 5.092$ Å, $c = 11.701$ Å and $\gamma = 90.387$

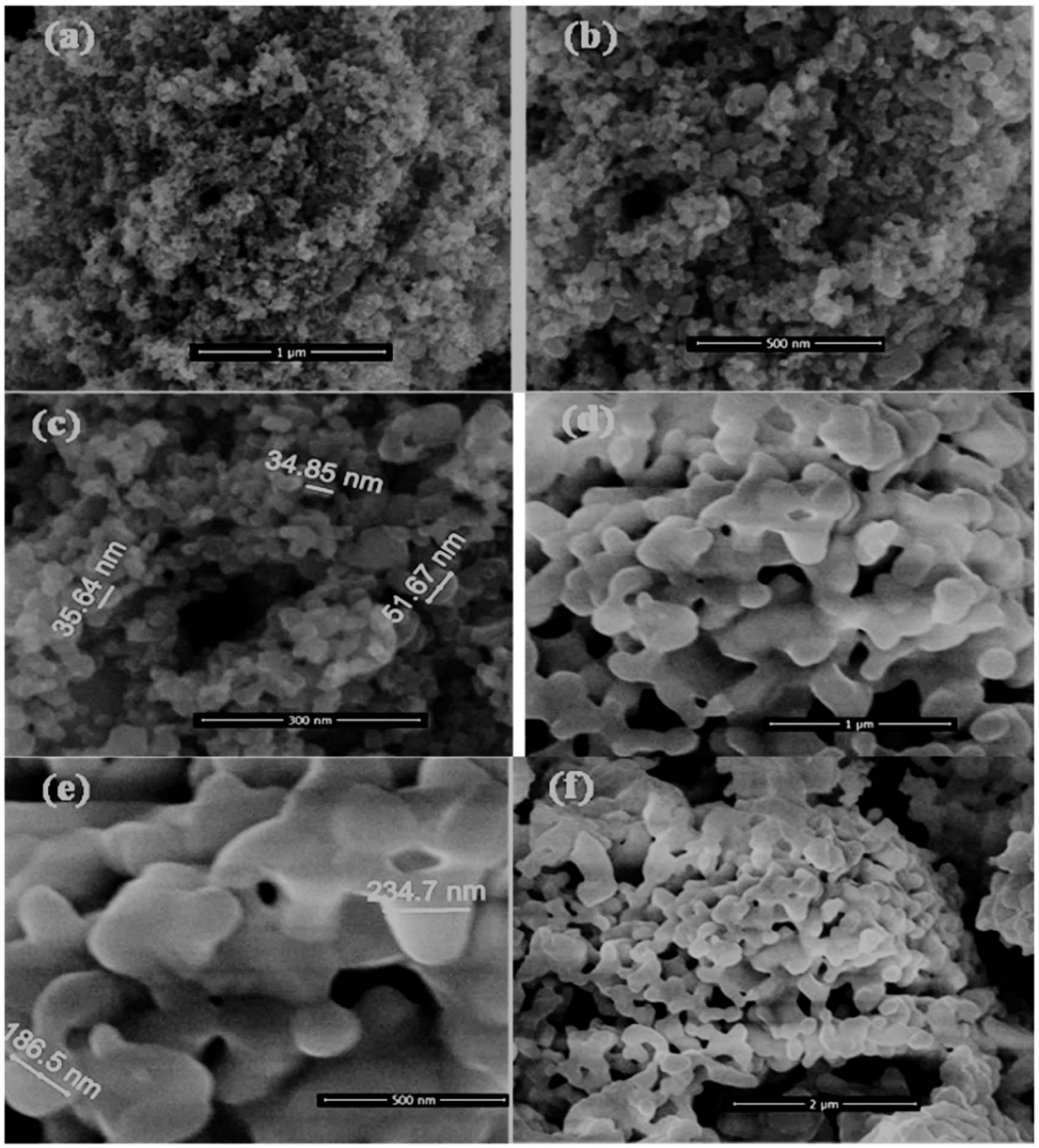

Fig. 1 SEM images of prepared nano-powders: (a–c) hydrogen peroxide modified titania; and (d–f) $BiVO_4$ powders calcined at 600 °C.

Å.[46] Fig. 3 shows that the diffraction peaks/planes of HMT and $BiVO_4$ simultaneously occurred in 15%$BiVO_4$@HMT samples; where no other impurity peaks have been detected which were attributed to the absence of contaminants in the impregnation (synthesis) process. The intensity of the predominant planes of $BiVO_4$ and HMT, such as (121) and (101), was reduced compared to the pristine samples. The findings can be attributed to the lattice alteration caused by the 'interfacial strain' between the $BiVO_4$ and HMT powders[47]

3.3. Elemental composition analysis

Energy dispersive X-ray analysis (EDAX) or EDS analysis was performed to identify elemental composition of samples. EDS of hydrogen peroxide modified titania shows, that elemental composition of crystal is free from any impurities (Fig. S2(a)†). The peak around 1 keV and 5 keV can be attributed to the crystal surface, where Ti are present in a smaller amount (due to formation of peroxo complexes), while an intense peak around 4.5 keV can be assigned to bulk of Ti[48] whereas, EDS analysis for $BiVO_4$ reveals that single phase constitutes bismuth (Bi), vanadium (V) and oxygen (O). In addition, calcination at temperature of 600 °C, the sharp peaks of vanadium in $BiVO_4$ structure are less intense compared to the sharp peaks of bismuth at 2.7 keV (Fig. S2(b)†). The peak intensities indicate that temperature affects the existence of elements in the crystal lattice and at the higher temperature bismuth is the more concentrated element (Table 1). These EDS results are in good agreement with the results reported by Longchin and co-workers.[45] Moreover, the energy values of specific X-ray radiations emitted by elements have been recorded as; for bismuth $L_\alpha = 10.84$, $L_\beta = 13.0$, $M_\alpha =$

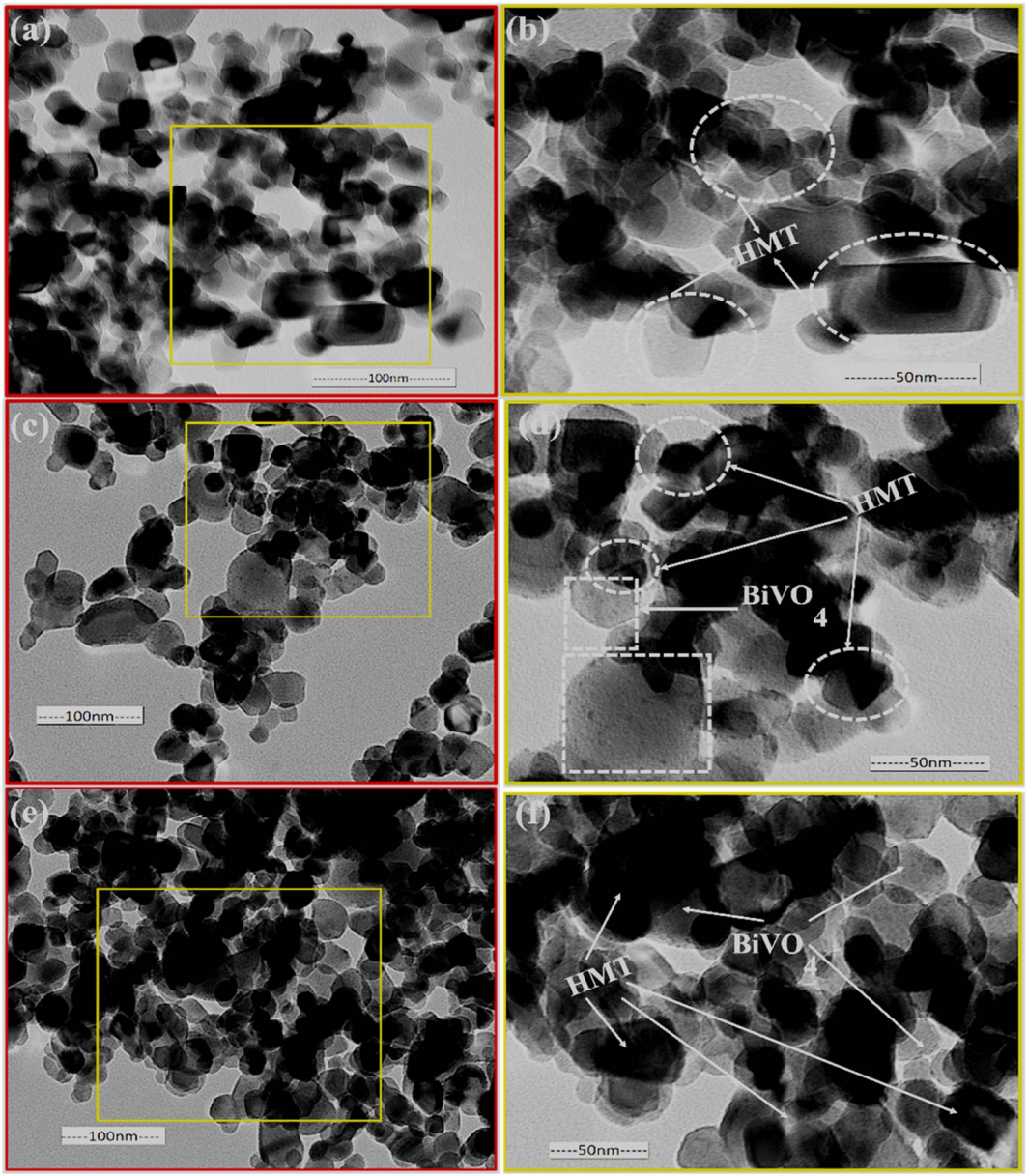

Fig. 2 TEM images of pristine TiO_2 (a and b); 10%$BiVO_4$@HMT (c and d) and 15%$BIVO_4$@HMT (e and f) nanocomposites.

2.42 and $M_\beta = 2.53$ keV; for vanadium, $K_\alpha = 4.95$, $K_\beta = 5.42$, $L_\alpha = 0.52$ and $L_\beta = 0.51$ keV while for oxygen $K_\alpha = 0.52$ keV.[38]

3.4. X-ray photoelectron spectroscopy analysis

The formation of composite was confirmed by X-ray photoelectron spectroscopy. Bi-5d, Bi-4f, C-1s, Bi-4d, Ti-2p, V-2p, O-1s were detected as obvious peaks in the survey spectrum of 15% $BiVO_4$@HMT (Fig. 4a). XPS signals for Bi-4f (Fig. 4b) at binding energies 164.5 eV and 159.4 eV were assigned to Bi-$4f_{5/2}$ and Bi-$4f_{7/2}$, this confirms the existence of Bi as Bi^{3+}.[49] Two binding energy peaks at 516.8 eV and 524.8 eV in the 15% composite of $BiVO_4$@HMT (Fig. 4c) were designated to V-$2p_{3/2}$ and V-$2p_{1/2}$ which can be ascribed to V^{5+} oxidation state of VO_4^{3-} in the sample.[50] while the peak detected at 530 eV was attributed to O-1s, originating from lattice oxygen.[51] The high resolution XPS spectra given in (Fig. 4d) depict the signals of Ti-2p in composite sample with binding energies of 458.5 eV and 464 eV for Ti-$2p_{3/2}$ and Ti-$2p_{1/2}$, respectively. At about 473 eV, a broad peak of Ti$\cdots$O shake-up satellite was recorded originating from ''shake-up' processes'', thus representing the bonding between Ti and O_2 species.[52] The O-1s peaks at 529.98 eV and shoulder peak at binding energy of 531.5 eV (Fig. 4e) pointed to the lattice oxygen atoms and the binding of Ti–O on sample surface, respectively.[53] When compared to the binding energies of O-1s in pure modified titania (data not shown here), which were 530.5 eV and 532.3 eV, these were changed to 529.9 eV and 531.5 eV. The change in binding energies can be ascribed to the formation of a strong interface between $BiVO_4$ and HMT.[54] Signals of C-1s presented in Fig. 4f, where it was used for calibration. Signals

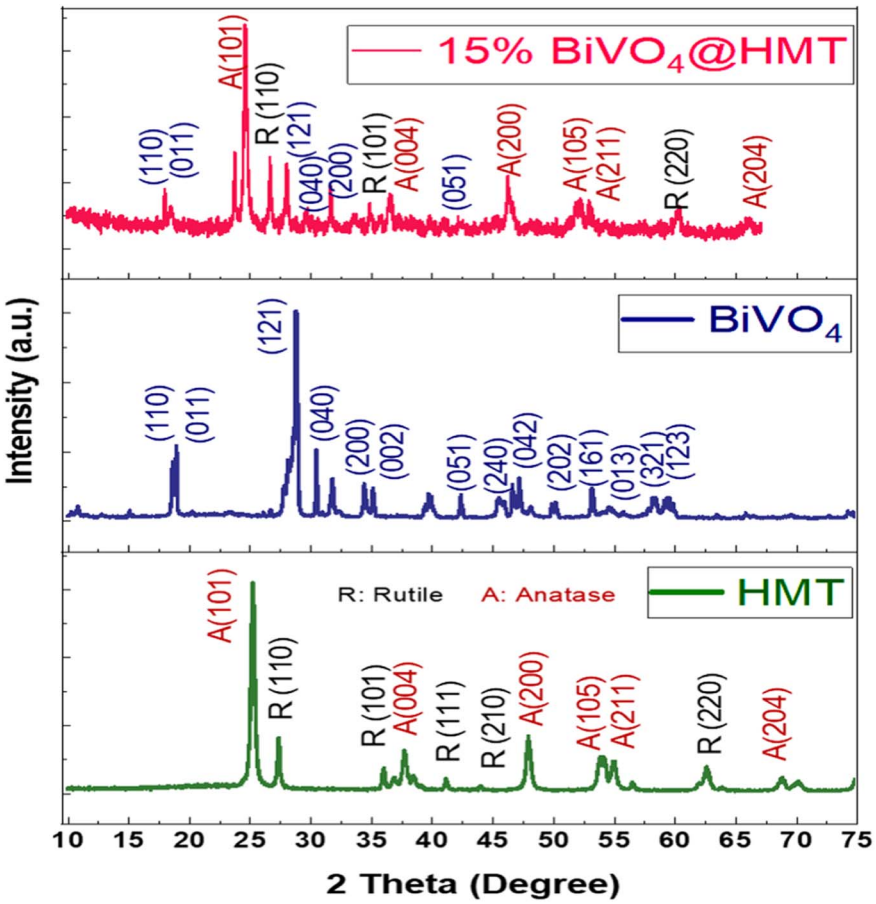

Fig. 3 XRD spectra of HMT, $BiVO_4$ and 15%$BiVO_4$@HMT.

Table 1 Comparison of elemental net intensities in $BiVO_4$ at different calcination temperatures

Element and shell name	Calcination Temperatures		
	400 °C	500 °C	600 °C
Bi (M)	191.32	220.89	271.01
V (K)	399.04	161.27	162.90
O (K)	22.36	17.90	8.87

of carbon in the form of sp^2 bonds usually originate at 284.8 eV while C-1s signals at 288.6 eV can be assigned to oxygen containing functional groups C═O, which arise from the carbon tape, used for XPS measurements.[52]

3.5. Optical properties and band gap analysis

Optical absorption properties are essential to characterise photocatalytic activity of samples and are believed to be critical in catalysts formulation. So, a UV-vis diffuse reflectance spectrum (DRS) was obtained to study the response of samples to light. As shown in Fig. 5a the 15%$BiVO_4$@HMT samples showed greater response to visible light in the 400 nm to 550 nm range (generating a yellowish-red shift) which indicates strong absorption towards visible light. In addition, the light absorbance efficiencies of nanocomposites were estimated from UV-visible reflectance spectra (Fig. 5a) using Kubelka–Munk ($F(R) = (1 - R)^2/(2R)$) relationship[35,52] which demonstrated that 15%$BiVO_4$@HMT composite have a higher light harvesting efficiency than other samples. The band gaps calculated from $(\alpha h\nu)^{1/2}$ *versus* $h\nu$ were assessed to be 3.2 eV, 3.1 eV and 2.9 eV, respectively, while 15% composite had a smaller band gap of 2.54 eV in comparison to the pure HMT, 1% and 5% composites (Fig. 5b). The decrease in the band gap can be explained by the formation of a heterojunction between the two components, which can be activated by absorbing visible light irradiation, thus generating more e^-/h^+ pairs, which will lead to greater inhibition of bacteria growth.

3.6. Microscopic morphology of cyanobacteria

For our study, a locally isolated culture of cyanobacteria was used. Samples observed at different magnifications (Fig. 6a–c) showed the outline of colony and the shape of the cells. Microscopic images revealed the presence of spherical cyanobacterial cells. At 100× magnification, the elliptical and globular gas vesicles, important for the cell/bloom buoyancy, were visible, as they constitute a major part of cyanobacterial cells. These morphological revelations were consistent with studies reporting microscopic observations of *Microcystis* specie.[55]

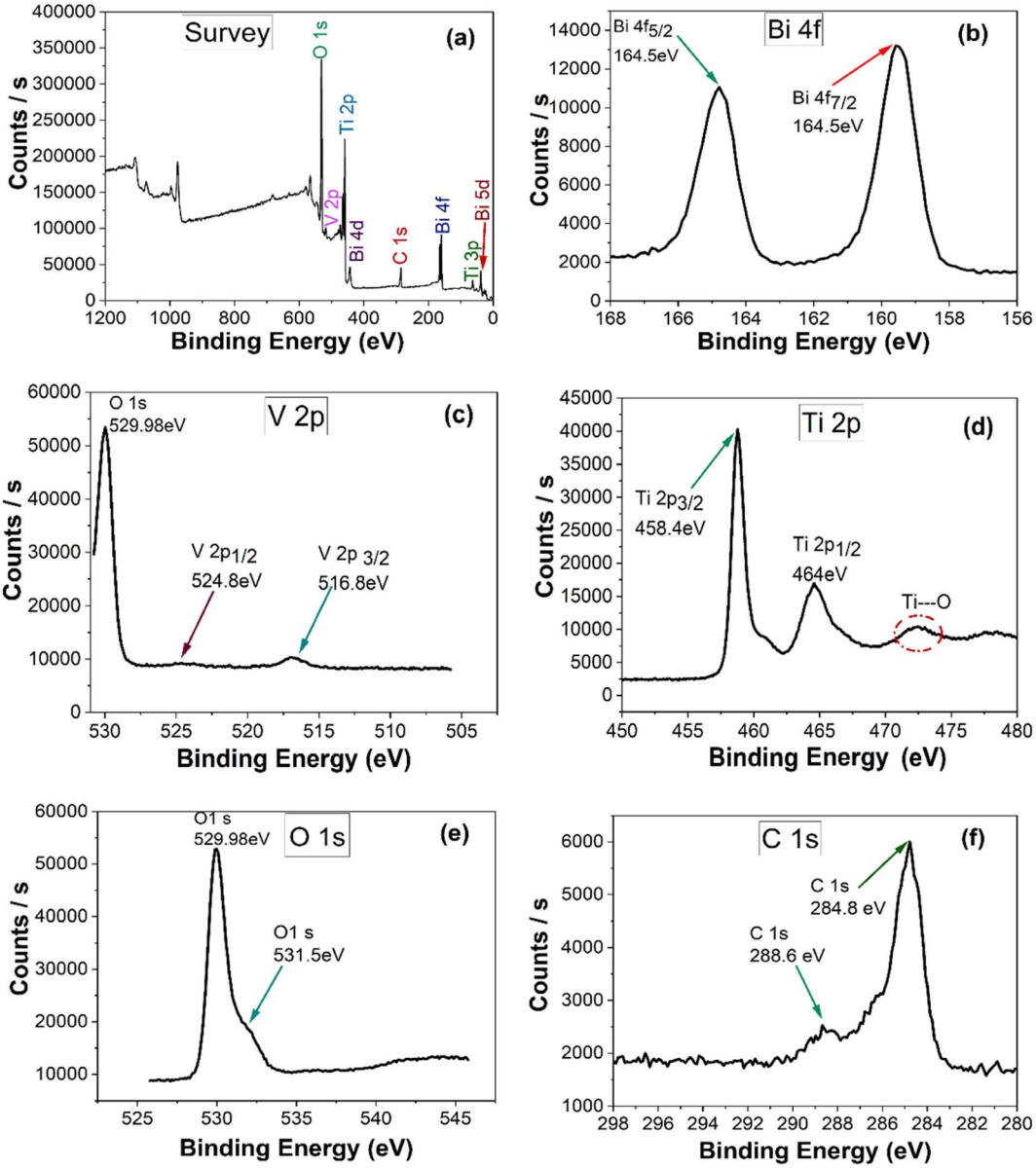

Fig. 4 (a) XPS survey scan and high resolution XPS spectra of (b) Bi-4f; (c) V-2p; (d) Ti-2p; (e) O-1s; (f) C-1s of 15%$BiVO_4$@HMT composite.

3.7. Effect of pH on the growth of cyanobacteria

Generally, variations in aquatic system pH and dominant carbon species alter the plankton's community, in case of cyanobacteria; the alkaline pH (low CO_2 concentrations) promotes their growth in the context of the 'Carbon capturing mechanism' (CCM). CCM involves five carbon uptake systems, including CO_2 uptake systems NDH-I_3 and NDH-I_4 and three bicarbonate uptake systems and transporters SbtA, BicA and Bct1. With these three systems of CCM, cyanobacteria tend to capture the carbon in HCO_3^- form *via* 'symporters' (transporter for Na^+/HCO_3^-) on the cell membrane. HCO_3^- ions enter the carboxysome, where the carbonic anhydrase enzyme dehydrates them back to CO_2. In this compartment, CO_2 is concentrated together with enzyme Rubisco for the process of photosynthesis, thus increasing the content of chlorophyll '*a*', which is necessary for cell division.[56,57] Our study demonstrates, that upon incubation at different pH ranges, the increase in chlorophyll '*a*' content in acidic medium is limited even on the 20th day of incubation, while under neutral and basic conditions, the growth reached a maximum between pH 8–10 (Fig. 7a). It then started to decrease at pH 11 and again expressed a dramatic decline at pH 12 (Fig. 7a). These results suggested that an alkaline pH in the range from 8 to 10 is the optimum pH (pH 8 also in case of control setup) for cyanobacterial growth, and these results are consistent with the findings of other researchers.[56,58,59]

The poor cyanobacterial growth at pH 11 and 12 (Fig. 7a) can be explained by the absence of CO_3^{-2} transporters in system; moreover, at pH 12 and >12, CO_2 become the dominant species, again, which reduces the activity of carbonic anhydrase. It is the

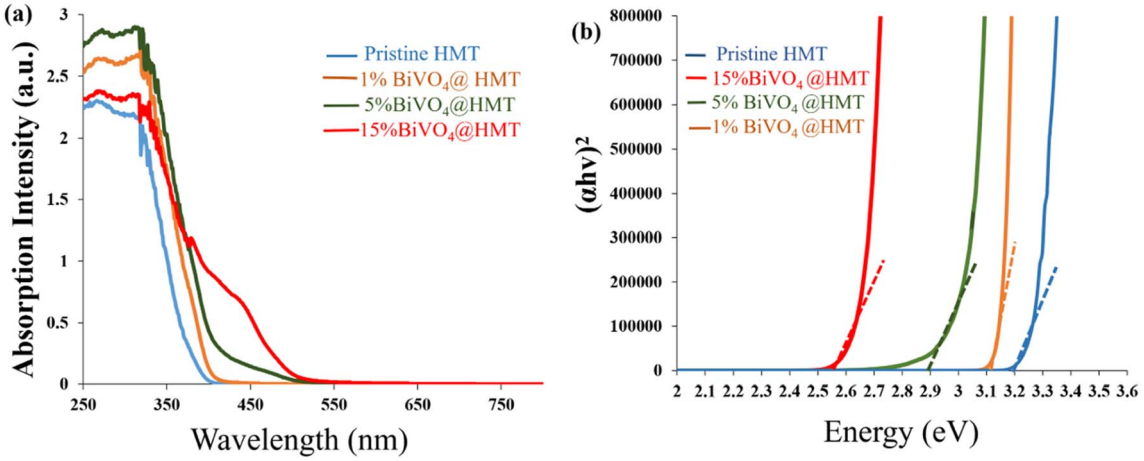

Fig. 5 (a) UV-vis diffuse reflectance spectra pure HMT, 1%$BiVO_4$@HMT, 5%$BiVO_4$@HMT and 15%$BiVO_4$@HMT; (b) Tauc plots of HMT, 1% $BiVO_4$@HMT, 5%$BiVO_4$@HMT and 15%$BiVO_4$@HMT

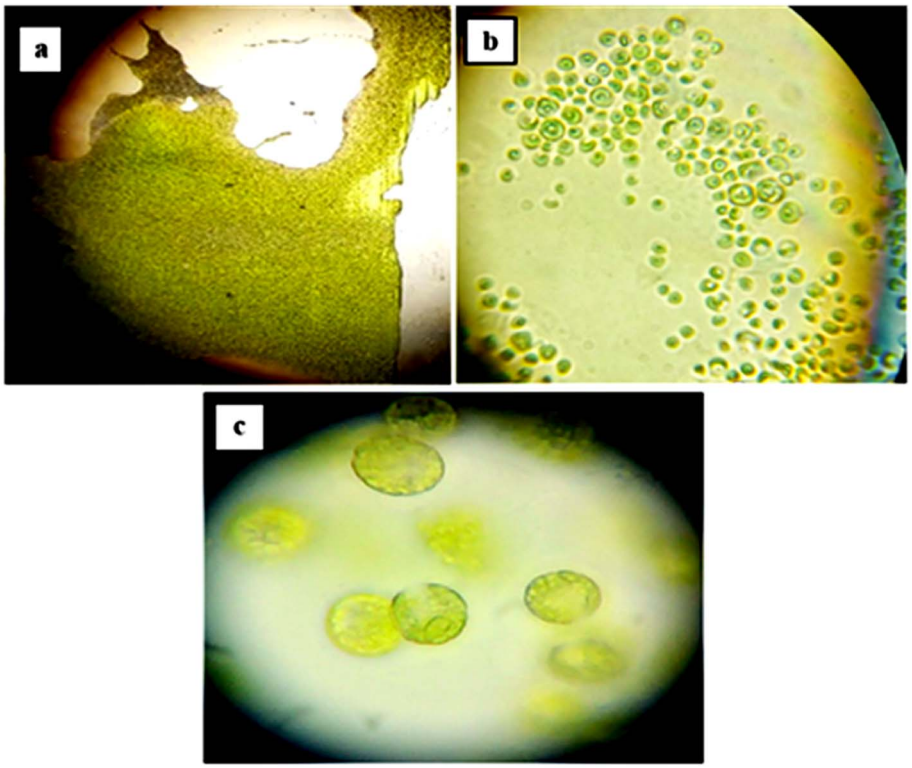

Fig. 6 Microscopic morphology of cyanobacterial culture at different magnifications; (a) 10× magnification; (b) 40× magnification; (c) 100× magnification.

same in the case with acidic pH, where an excess of CO_2 and H^+ ions inhibited the cyanobacterial growth by reducing enzymatic activity and disrupting the functioning of CCM. Acidic surroundings also acidifies the inner environment of algal cell, which denatures the photosystem II (PSII) of photosynthetic machinery, affects cellular cytoplasm, which stops the Calvin–Benson cycle resulting to PSII reactions termination.[60] pH 5 and 6 starts to affect ribulose-1,5-bisphosphate (RUBP) thus affecting the photosynthetic activity (loss in O_2 evolution). It has also proposed that low pH (especially pH < 5) affects the cell membrane and its transporters. The damage to the transporters due to acidic environs effects the availability of nutrients and co-factors resulting to loss in production and replication of DNA, RNA which eventually stops the protein synthesis; consequently, leading to cell death and growth inhibition.[61,62] Cells growth in our results at pH 6 can be attributed to the presence of Ca^+ ions in cells adsorbed from growth media; which help them to stay resilient at slightly acidic conditions

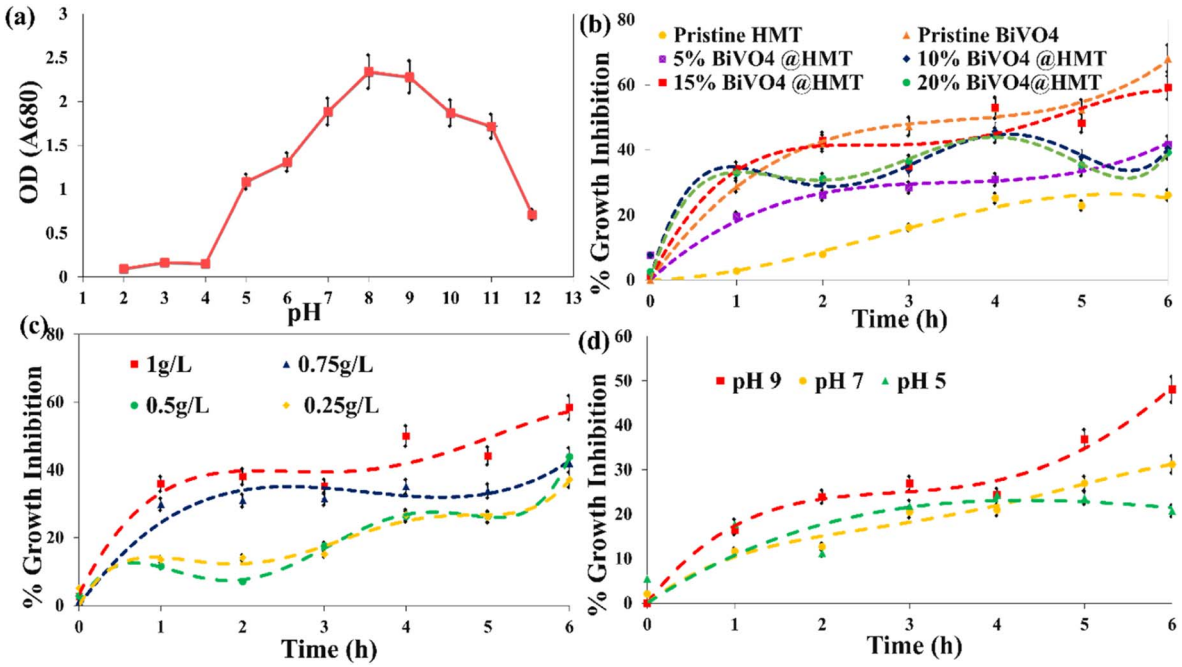

Fig. 7 (a) Effect of pH on the growth of cyanobacteria incubated at different pH for 20 days; (b) growth inhibition by pristine and composite photocatalyst (catalyst dose 1 g L^{-1}, algal concentration 0.1 g L^{-1}, pH 6.9); (c) effect of 15%$BiVO_4$@HMT dose on growth inhibition (algal concentration 0.1 g L^{-1}, pH 6.9); (d) effect of the pH of the solution on growth inhibition activity of 15%$BiVO_4$@HMT (algal concentration 0.1 g L^{-1}; catalyst dose 1 g L^{-1}).

(pH = 6), where they can maintain their physiological processes.[63] In summary, the results show that cyanobacteria have a greater potential to grow in alkaline environment due to their efficient CCM. Moreover, slightly alkaline conditions and climate change has altered and evolved cyanobacteria to outcompete other phytoplankton. In acidic condition, they can't proliferate and can't compete with green algae, that's why cyanobacteria are uncommon in an acidified lake.

3.8. Photocatalytic inhibition of the growth of cyanobacteria

3.8.1. Effect of catalyst variation on inhibition of the growth of cyanobacteria. Pristine $BiVO_4$ powders have shown the highest activity for the inhibition of growth of cyanobacteria compared to pure HMT, where the former catalyst inhibition percentage was about 68% while the later showed only about 26% decline in growth of algae (Fig. 7b). Preparing the composites of pristine HMT with $BiVO_4$ improved its catalytic activity. The descending order of the catalytic activity was observed as $BiVO_4$ > 15%$BiVO_4$@HMT > 10%$BiVO_4$@HMT > 20%$BiVO_4$@HMT = 5%$BiVO_4$@HMT > HMT, respectively. However, when compared to 15% and 10% nanocomposites, 20%$BiVO_4$@HMT expressed lower growth inhibition efficiency (Fig. 7b) possibly due to agglomeration of impregnated component which lead to lowered numbers of active sites, consequently, lessened harvesting of incoming irradiation.[52,64]

Although it was previously reported that TiO_2 modified with H_2O_2 is an efficient photocatalyst[64–66] this was not applied for these experiments on inhibition of growth of cyanobacteria. It had a lower catalytic activity compared to other nanocomposites. This can be associated either with the recombination of e^-/h^+ pairs or with the adsorption of cellular debris on the catalyst surface, which reduce the activity of HMT catalyst.[67] The greater inhibition of growth in the case of 15% $BiVO_4$@HMT composite can be due to appropriate deposition of a large amount of $BiVO_4$ on the HMT powders and formation of a heterojunction, which provides efficient charge separation.

3.8.2. Effect of catalyst dose on cyanobacterial growth inhibition. The effect of catalyst loading is an important factor in the case of photocatalysis used to decompose organic pollutant.[52] With an increase in the catalyst dose of 15% $BiVO_4$@HMT from 0.25 g L^{-1} to 1 g L^{-1}, the percentage of cell degradation increased (Fig. 7c). The inhibition efficiencies of the composite photocatalyst were 37%, 43% and 58% for 0.25 g L^{-1}, 0.5 g L^{-1} and 1 g L^{-1} dose, respectively. This may be due to an increase in active sites due to an increased in the dose and a greater formation of reactive oxidation species (ROS), which is the result of increased absorption of light by catalysts. It is evident from the results that a greater inhibition effect was observed at 1 g L^{-1} for 15%$BiVO_4$@HMT in visible light, therefore it was used for the following experiments.

3.8.3. Effect of solution pH on photocatalytic cyanobacterial inhibition. In heterogeneous photocatalysis, the pollutant degradation also depends on the pH of the solution, as it plays a crucial role by modifying the surface of both, the catalyst and the pollutants. For this purpose, three pH ranges; 5, 7 and 9 were chosen because too low and too high pHs have not been reported to be compatible with the CCM of cyanobacteria, as discussed in detail earlier (Section 3.7). So, the growth inhibition activity of 15%$BiVO_4$@HMT increased with increase of pH in the order pH 9 > pH 7 > pH 5 (Fig. 7d), which could be

explained by following. Increased growth inhibition or cell rupture at alkaline pH can be explained by the production of ROS (in bulk) followed by attacks on organic bonds (C–C, C–H, C–N, C–O, H–O), damaging the bilipid layer of cells and degrading proteins that got exposed to external environment. This significantly altered the molecules in cells and lead to cell wall leakage and cell death.[68,69] Another explanation for the increased inhibition of growth at alkaline pH can also be confirmed by the fact of their ability to uptake HCO_3^- at alkaline pH. In the present study, the harvested biomass was stored in a refrigerator to avoid any contamination, so the cells suffered from starvation. When they were exposed to alkaline pH and visible light, cells began to develop positive zeta potential by utilizing proton motive force (PMF) to capture HCO_3^- ions by the stimulating Na^+/H^+ antiporters. The zero charge (pH_{PZC}) point of 15%$BiVO_4$@HMT was calculated to be 5.25 using the 'salt addition method'[25] using 0.1 M KCl solution. This indicates the presence of a positive charge on the catalyst surface below pH_{PZC} and a negative charge at a pH above pH_{PZC}. So, the accumulation of a positive charge on the cell surface forces the cells to approach the negatively charged photocatalyst,[70–72] which led to increased inhibition of growth.

3.8.4. Mechanism route for photocatalytic activity. Based on the results of physico-chemical characterizations and photocatalytic growth inhibition performance, the plausible route for algal cell denaturation using as-synthesized 15%$BiVO_4$@HMT was proposed. Fig. 7b displays higher growth inhibition *via* 15%$BiVO_4$@HMT, it can be stated that this catalyst have comparatively enhanced light absorption capacity owing to its smaller bandgap, therefore, more electron–hole pairs created over the heterojunction. So, Fig. 8 demonstrates the junction formation between 15%$BiVO_4$@HMT as of type-II like positioning, depicting that upon absorption of visible light, electrons from the VB of $BiVO_4$ and HMT got excited and transferred in their respective CBs, followed by rapid recombination of photogenerated electrons in HMT's CB with photogenerated holes in $BiVO_4$'s VB, leaving the higher energy electrons and holes at more negative and more positive potentials with enhanced redox capabilities. This prescribed mechanism is in good coherence with the scavenging studies (Fig. S5(b)†) suggested that holes and electrons have major contribution among other ROSs, which was margined separately for direct oxidation and reduction at higher potentials, thus leading to cell damage. However, it will be truly to say that heterojunction formation improved the exploitation of light and halted the recombination of charge carriers at $BiVO_4$@HMT interface; whereas the photocatalytic activity order of 15%$BiVO_4$@HMT is; no-scavenger > $OH^\bullet$ > $O_2^{\bullet-}$ > e^- > h^+ (Fig. S5(b)†).

3.8.5. Effect of photocatalysis on cyanobacterial cell and chlorophyll '*a*'. Two possibilities have been proposed to explain the anti-microbial or anti-algal activities of nanoparticles. Initially, when cells meet nanoparticles, former are taken-up/adsorbed by later or *vice versa*, where they are involved in inhibiting enzymatic and metabolic activities, causing serious damage to the cells. Secondly, production of ROS due to activation of catalyst by absorbing visible light (eqn (2)–(7)) that have caused cell wall damages and let the cells leak their contents owing to irretrievable lost integrity and lethal modifications. These attacks become continuous due to efficient charge separation as it trends in a Z-scheme junction[32] which are powerful enough to inactivate or kill cyanobacterial cells.[73] Algal growth to be steadily declining compared to negative control sets. The pigment absorption decreases from 0.0385 to 0.01685 after 6 h and at 1 g L^{-1} of catalyst. So, based on the decrease in chl '*a*' content, it can be assumed that when catalysts were added to a cell suspension of 0.1 g L^{-1}, it interacted with cells (Fig. S3 and S4†) and produced ROS which started to attack cell wall constituents which are vulnerable to radical

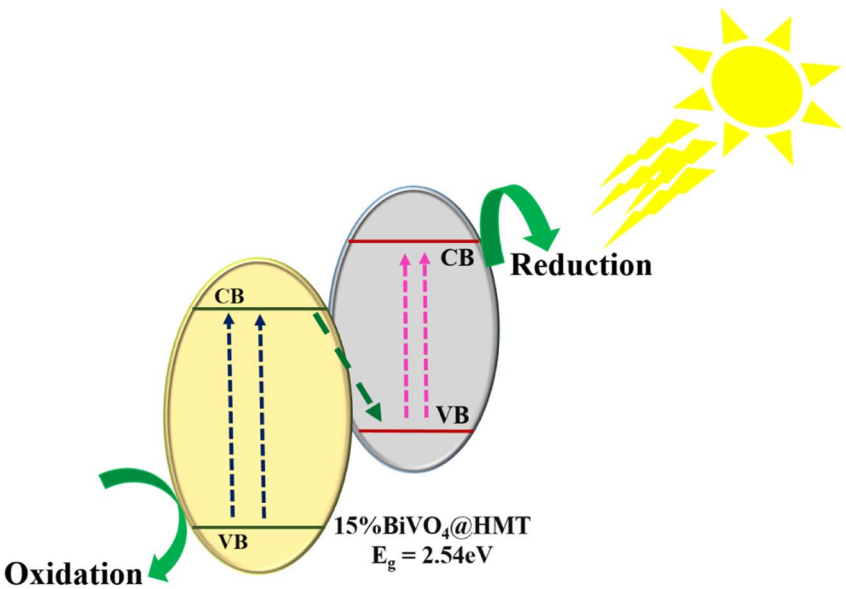

Fig. 8 Schematic illustration of photocatalytic activity of 15%$BiVO_4$@HMT under visible light.

attacks such as; 'L-α-phosphatidylethanolamine' (L-α-cephaline or PE).[74] Continuous attacks by ROS (say, h^+) on cell inclusions also induced a lot of damages to the chl '*a*' structure. Moreover, photosynthesis is reported to be stopped directly when organelles and photosynthetic machinery (photo-systems) are exposed to an environment with excessive amount of ROS, followed by the decreasing absorbance of pigment due to breakage of the head and tail structure of Chl '*a*'.[22,75,76] From the results presented in (Fig. 7c), the percentage of growth inhibition is visibly bit static and does not decline rapidly until the 3rd and 4th h of photocatalytic process. This behaviour can be explained by the activation of the defence mechanism of cyanobacterial cells. Since blue-green alga are Gram negative, their defence system comprises of the catalase enzyme (CAT) and super oxide dismutase (SOD), where H_2O_2 decomposes into water and oxygen and thus they convert the superoxide radical into an oxygen molecule. After the 5th and 6th h of photocatalytic exposure, the inhibition efficiency increased rapidly, which may indicate that the ROS production in the experimental system surpassed the ability of antioxidants to protect cells (Fan *et al.*,[76] 2019b). The proposed mechanism for generation of ROS and attacks on cell is given in eqn (2)–(7):

$$15\%BiVO_4@HMT + h\nu \rightarrow h^+ + e^- \quad (2)$$

$$h^+ + H_2O \rightarrow {}^{\bullet}OH + H^+ \quad (3)$$

$$e^- + O_2 \rightarrow O_2^{\bullet -} \quad (4)$$

$$O_2^{\bullet -} + H^+ \rightarrow HOO^{\bullet} \quad (5)$$

$$e^- + HOO^{\bullet} + H^+ \rightarrow H_2O_2 \quad (6)$$

$$H_2O_2 + e^- \rightarrow OH^{\bullet} + OH^- \quad (7)$$

So, it is postulated that cellular rupture started with the photocatalytic action of catalyst, production of ROS, initiating the 'radical induced changes' in defence structures such as phospholipids and polysaccharides in the cell wall and membrane, and then caused oxidative damage to chl '*a*' and other structures.[77]

3.9. Comparison of catalyst activities from literature

A number of studies have been carried out on the anti-algal activities of nanoparticles[78–81] where the nanoparticles shown promising results in inhibiting algal/cyanobacterial growth by

Table 2 Comparison of catalyst activities for algal growth inhibition from literature

Nanomaterial type	Cell/specie type	% Growth inhibition	Reaction time	References
15%$BiVO_4$@HMT NPs	Locally isolated cyanobacteria	59%, under visible light	6 h	Present study
Ag_2CO_3–GO nanoparticles	*Microcystis aeruginosa*	Nearly 100%, using visible light	7 h	65
Floating g-C_3N_4 heterojunction on EP/Al_2O_3 nanoparticles	*Microcystis aeruginosa*	74.4%, using visible light	6 h	68
Ag/AgCl@ZIF-8 nanoparticles	*Microcystis aeruginosa*	98.5%, using visible light	4 h	76
0.2% PDDA@NPT-EGC (poly dimethyl diallyl ammonium chloride (PDDA)@N–P co-doped TiO_2/expanded graphite C/C floating composite (NPT-EGC)	*Microcystis aeruginosa*	77%, using visible light	2 h	77
Zn–Fe LDHs nanoparticles	*Microcystis aeruginosa*	80%, using visible light	3 h	78
TiO_2, WO_3 with Pt Co-catalyst	Algae	87%, under florescent lamps	—	80
$AgBiO_3$ nanoparticles	*Microcystis aeruginosa*	72.2%, using visible light	4 h	82
Fe_3O_4–TiO_2 core/shell magnetic NPs	*Streptococcus pyogenes*	85%, UV-light	20 min	83
TiO_2 nanoparticles	*Pseudomonas aeruginosa*	About 100% was achieved under UV light	50 min	84
TiO_2/Ag in chitosan nanocomposite films	*Dunaliella salina*	45%, under UV-C light	—	85
Fe_2O_3–TiO_2 nanoparticles	*Chlorella vulgaris*	99%, under visible light	24 h	86
CuONPs/GLYMO/4-HBPA	*Chlamydomonas reinhardtii*	99%, using visible light	—	87
3D Ag_2O/g-C_3N_4 hydrogel	*Microcystis aeruginosa*	98.8%, visible light	4 h	88
Ag/AgCl@g-C_3N_4@UIO-66(NH_2)	*Microcystis aeruginosa*	99.9%, visible light	3 h	89
Ag_2MoO_4/TACN@LF	*Microcystis aeruginosa*	100%, visible light	4 h	90

disrupting outer membranes and photosynthetic systems in comparison to several chemical control strategies. Some examples of growth inhibition (algal and non-algal) from the literature are given in Table 2.

4. Conclusion

In this study, we demonstrate that modification of HMT surface with 15% $BiVO_4$ was found to be effective in inhibiting algal growth compared to pure HMT and other composites. The co-occurrence of pristine nanoparticles with high crystallinity and the formation of a heterojunction due to creation of a lamellar arrangement of $BiVO_4$ in the composite was shown by XRD and TEM analysis. The established junction improved the overall reaction chemistry by preventing recombination of electrons/holes pairs, decreasing the band gap, and also by increasing the ability of nanoparticles to adsorb visible light with a subsequent increase in photocatalytic activity. The synthesized nanocomposite catalyst showed high growth inhibition efficiency at higher pH, where percentage inhibition was directly related to pH, and these results were in good synergy with the increased growth of cyanobacterial in alkaline environment. Moreover, the use of 15%$BiVO_4$@HMT for only 6 h was sufficient enough to induce the death of locally isolated cyanobacterial cells. The reactive oxygen species generated by the photocatalytic process were active enough to disrupt the protein complex of Chl '*a*', and indicated growth inhibition of up to 59%. We foresee the strong potential of this composite, which could potentially be applied to inhibit the growth and bloom of cyanobacteria to restore various water bodies by exploiting visible radiations. The materials could be also used in drinking water treatment plants to overcome the high turbidity and algal bloom problem that cause clogging the sand filters. The catalyst can also be used for simultaneous degradation of organic contaminants.

5. Future recommendations

✓ In regards of HABs control in real systems, development of target oriented photocatalysts is required which will only be capable of oxidizing harmful cyanobacterial cells rather than every cell being encountered. This tailoring will help in improved recovery of eutrophicated waters as well as preparation of budget friendly anti-algal nano-supplies.

✓ Only limitation associated to the use of nanocatalysts, which is present and addressed in literature, is the recovery, separation and recycling problem specially after anti-algal treatment, where catalyst recovery with adsorbed dead cells from bottom of suspension has been an issue, thus leading to wastage of NPs' and being cost intensive. There is need to devise such a system which should have potential to overcome this difficulty.

✓ There is a room to create extended research scopes for the degradation of DNA, RNA, proteins or amino acids molecules which will add fruitful perspectives in the cell denaturation mechanism.

Data availability

The datasets supporting this article have been uploaded as part of the ESI.†

Author contributions

Jamshaid Rashid: conceptualization, supervision, material characterization, original draft preparation, manuscript revision and editing. Fatima Imtiaz: data curation, methodology, experimentation, writing – original draft preparation. Ming Xu: characterization support, writing – reviewing and editing. Irina Savina: writing – reviewing and language editing.

Conflicts of interest

The authors declare that they have no known competing financial interests or personal relationships that could have appeared to influence the work presented in this paper.

Acknowledgements

The authors acknowledge Quaid-i-Azam University for funding this research and Dr Ming Xu for extending his courtesy in performing characterizations.

References

1 J. C. Ho, A. M. Michalak and N. Pahlevan, *Nature*, 2019, **574**, 667–670, DOI: **10.1038/s41586-019-1648-7**.
2 W. A. Wurtsbaugh, H. W. Paerl and W. K. Dodds, *Water*, 2019, **6**, e1373, DOI: **10.1002/wat2.1373**.
3 D. P. Holland, A. Pantorno, P. T. Orr, S. Stojkovic and J. Beardall, *Water Res.*, 2012, **46**, 1430–1437, DOI: **10.1016/j.watres.2011.11.015**.
4 T. T. Duong, T. P. Q. Le, T.-S. Dao, S. Pflugmacher, E. Rochelle-Newall, T. K. Hoang, T. N. Vu, C. T. Ho and D. K. Dang, *J. Appl. Phycol.*, 2013, **25**, 1065–1075, DOI: **10.1007/s10811-012-9919-9**.
5 M. Lürling, F. Van Oosterhout and E. Faassen, *Toxins*, 2017, **9**, 1–16, DOI: **10.3390/toxins9020064**.
6 B. Bakheet, M. A. Islam, J. Beardall, X. Zhang and D. McCarthy, *Chem. Eng. J.*, 2018, **350**, 616–626, DOI: **10.1016/j.cej.2018.06.012**.
7 M. Skafi, S. Vo Duy, G. Munoz, Q. T. Dinh, D. F. Simon, P. Juneau and S. Sauvé, *Toxicon*, 2021, **194**, 44–52, DOI: **10.1016/j.toxicon.2021.02.004**.
8 J. Park, J. Church, Y. Son, K.-T. Kim and W. H. Lee, *Ultrason. Sonochem.*, 2017, **38**, 326–334, DOI: **10.1016/j.ultsonch.2017.03.003**.
9 M. Lürling and W. Beekman, *J. Appl. Phycol.*, 2010, **22**, 503–510, DOI: **10.1007/s10811-009-9485-y**.
10 I. Priyadarshani, N. Thajuddin and B. Rath, *Int. J. Curr. Microbiol. Appl. Sci.*, 2014, **3**, 173–182.
11 H. C. P. Matthijs, D. Jančula, P. M. Visser and B. Maršálek, *Aquat. Ecol.*, 2016, **50**, 443–460, DOI: **10.1007/s10452-016-9577-0**.

12 S. E. Coloma, A. Dienstbier, D. H. Bamford, K. Sivonen, E. Roine and and T. Hiltunen, *Environ. Microbiol.*, 2017, **19**, 273–286, DOI: **10.1111/1462-2920.13601**.
13 K. K. DeRose, R. W. Davis, E. A. Monroe and J. C. Quinn, *J. Great Lakes Res.*, 2021, **47**, 1021–1032, DOI: **10.1016/j.jglr.2021.04.011**.
14 P. Rajasekhar, L. Fan, T. Nguyen and F. A. Roddick, *Water Res.*, 2012, **46**, 4319–4329, DOI: **10.1016/j.watres.2012.05.054**.
15 S. Banerjee, R. R. Sarkar and J. Chattopadhyay, *J. Theor. Biol.*, 2019, **469**, 61–74, DOI: **10.1016/j.jtbi.2019.02.016**.
16 D. Aryal, *Evaluating The Effectiveness Of Algaecide In A Continuous Flow Through System*, University of Akron, 2018.
17 C. P. Urrutia, M. K. Ekvall and L. A. Hansson, *PLoS One*, 2016, **11**, e0153032, DOI: **10.1371/journal.pone.0153032**.
18 M. Søndergaard, T. L. Lauridsen, L. S. Johansson and E. Jeppesen, *Water*, 2017, **9**, 43, DOI: **10.3390/w9010043**.
19 J. Rashid, F. Imtiaz and M. Xu, *Concepts of Semiconductor Photocatalysis*, IntechOpen, London, UK, 2019, vol. 2, pp. 9–58, DOI: **10.5772/intechopen.86542**.
20 Z. Zhu, J. Li, W. Li, X. Liu, Y. Dang, T. Ma and C. Wang, *Environ. Sci.: Nano*, 2022, **9**(5), 1738–1747, DOI: **10.1039/D2EN00050D**.
21 G. Fan, J. Zhou, X. Zheng, J. Luo, L. Hong and F. Qu, *Chemosphere*, 2020, **239**, 124721, DOI: **10.1016/j.chemosphere.2019.124721**.
22 H. Wang, X. Li, X. Zhao, C. Li, X. Song, P. Zhang and P. Huo, *Chin. J. Catal.*, 2022, **43**, 178–214, DOI: **10.1016/S1872-2067(21)63910-4**.
23 L. Zhou, M. Cai, X. Zhang, N. Cui, G. Chen and Z. G. Yan, *Appl. Catal., B*, 2020, **272**, 119019, DOI: **10.1016/j.apcatb.2020.119019**.
24 S. Kang, L. Zhang, C. Liu, L. Huang, H. Shi and L. Cui, *Int. J. Electrochem. Sci.*, 2017, **12**, 5284–5293, DOI: **10.20964/2017.06.54**.
25 J. Rashid, M. Barakat and N. Salah, *RSC Adv.*, 2014, **4**, 56892–56899, DOI: **10.1039/C4RA12990C**.
26 F. Gongduan, Z. Jiajun, L. Jing, Z. Jin, C. Zhong and Y. You, *Catal. Sci. Technol.*, 2019, **9**, 4614–4628, DOI: **10.1039/C9CY00965E**.
27 V. Dutta, S. Sharma, P. Raizada, R. Kumar, V. K. Thakur, V. H. Nguyen, A. M. Asiri, A. A. P. Khan and P. Singh, *J. Environ. Chem. Eng.*, 2020, **8**, 104505, DOI: **10.1016/j.jece.2020.104505**.
28 W. Li, X. Liu, X. Chu, F. Wang, Y. Dang, T. Ma, J. Li and C. Wang, *Environ. Sci.: Nano*, 2021, **8**, 3655–3664, DOI: **10.1039/D1EN00801C**.
29 M. Balamurugan, G. Yun, K.-S. Ahn and S. H. Kang, *J. Phys. Chem. C*, 2017, **121**, 7625–7634, DOI: **10.1021/acs.jpcc.6b12516**.
30 X. Meng and Z. Zhang, *J. Mol. Catal. A: Chem.*, 2016, **423**, 533–549, DOI: **10.1016/j.molcata.2016.07.030**.
31 D.-L. Guan, C.-G. Niu, X.-J. Wen, H. Guo, C.-H. Deng and G.-M. Zeng, *J. Colloid Interface Sci.*, 2018, **512**, 272–281, DOI: **10.1016/j.jcis.2017.10.068**.
32 A. Ebrahimi, N. Jafari, K. Ebrahimpour, M. Karimi, S. Rostamnia, A. Behnami, R. Ghanbari, A. Mohammadi, B. Rahimi and A. Abdolahnejad, *Ecotoxicol. Environ. Saf.*, 2021, **210**, 111862, DOI: **10.1016/j.ecoenv.2020.111862**.
33 P. Pookmanee, S. Kojinok and S. Phanichphant, *J. Met., Mater. Miner.*, 2012, **22**, 49–53.
34 J. Rashid, M. A. Barakat, N. Salah and S. S. Habib, *RSC Adv.*, 2014, **4**, 56892–56899, DOI: **10.1039/C4RA12990C**.
35 P. Norouzzadeh, K. Mabhouti, M. M. Golzan and R. Naderali, *Appl. Phys. A: Mater. Sci. Process.*, 2020, **126**, 1–13, DOI: **10.1007/s00339-020-3335-9**.
36 T. Zavřel, M. A. Sinetova and J. Červený, *Bio Protoc.*, 2015, **5**, 1–5, DOI: **10.21769/BioProtoc.1467**.
37 T. T. Duong, T. S. Le, T. Thu, H. Tran, T. K. Nguyen, C. T. Ho, T. H. Dao, T. Phuong, Q. Le, H. C. Nguyen, D. K. Dang, T. Thu, H. Le and P. T. Ha, *Adv. Nat. Sci.: Nanosci. Nanotechnol.*, 2016, **7**, 035018, DOI: **10.1088/2043-6262/7/3/035018**.
38 P. Pookmanee, S. Kojinok, R. Puntharod and S. Phanichphant, *Ferroelectrics*, 2013, **0193**, 45–54, DOI: **10.1080/00150193.2013.846197**.
39 S. Ali and M. A. Farrukh, *J. Chin. Chem. Soc.*, 2018, **65**, 276–288, DOI: **10.1002/jccs.201700163**.
40 M. F. R. Samsudin, S. Sufian, R. Bashiri, N. M. Mohamed and R. M. Ramli, *J. Taiwan Inst. Chem. Eng.*, 2017, **81**, 305–315, DOI: **10.1016/j.jtice.2017.09.045**.
41 E. Han, K. Vijayarangamuthu, J. Youn, Y. Park and S. Jung, *Catal. Today*, 2018, **303**, 305–312, DOI: **10.1016/j.cattod.2017.08.057**.
42 S. Kang, L. Zhang, C. Liu, L. Huang, H. Shi and L. Cui, *Int. J. Electrochem. Sci.*, 2017, **12**, 5284–5293, DOI: **10.20964/2017.06.54**.
43 S. Ko, J. Pekarovic, P. D. Fleming and P. Ari-gur, *Mater. Sci. Eng., B*, 2010, **166**, 127–131, DOI: **10.1016/j.mseb.2009.09.023**.
44 K. Manikandan, A. J. Ahamed, A. Thirugnanasundar and G. M. Brahmanandhan, *Dig. J. Nanomater. Biostructures*, 2015, **10**, 1427–1437.
45 P. Longchin, P. Pookmanee, S. Satienperakul, S. Sangsrichan, R. Puntharod, W. Kangwansupamonkon, S. Phanichphant, P. Pookmanee, S. Satienperakul, S. Sangsrichan and R. Puntharod, *Integr. Ferroelectr.*, 2016, **175**, 18–24, DOI: **10.1080/10584587.2016.1199845**.
46 A. H. Abdullah, N. M. Ali, M. Ibrahim and M. Tahir, *Malaysian J. Anal. Sci.*, 2009, **13**, 151–157.
47 J. Hu, J. Tu, X. Li, Z. Wang, Y. Li, Q. Li and F. Wang, *Nanomaterials*, 2017, **7**, 336, DOI: **10.3390/nano7100336**.
48 S.-H. Nam, T. K. Kim and J.-H. Boo, *Catal. Today*, 2012, **185**, 259–262, DOI: **10.1016/j.cattod.2011.07.033**.
49 Q. Su, L. Zhu, M. Zhang, Y. Li, S. Liu, J. Lin, F. Song, W. Zhang, S. Zhu and J. Pan, *ACS Appl. Mater. Interfaces*, 2021, **13**(28), 32906–32915, DOI: **10.1021/acsami.1c05117**.
50 R. A. Rather, M. Khan and I. M. C. Lo, *J. Catal.*, 2018, **366**, 28–36, DOI: **10.1016/j.jcat.2018.07.027**.
51 I. J. Tadeo, D. Bhardwaj, D. Sheela, S. B. Krupanidhi and A. M. Umarji, *J. Mater. Sci.: Mater. Electron.*, 2020, **31**, 4687–4695, DOI: **10.1007/s10854-020-03023-4**.
52 J. Rashid, A. Abbas, L. C. Chang, A. Iqbal, I. U. Haq, A. Rehman, S. Awan, M. Arshad and M. Rafique, *Sci. Total*

Environ., 2019, **665**, 668–677, DOI: 10.1016/j.scitotenv.2019.02.145.
53 H. Li, H. Yu, X. Quan, S. Chen and H. Zhao, *Adv. Funct. Mater.*, 2015, **25**, 3074–3080, DOI: 10.1002/adfm.201500521.
54 Y. Zhang, M. Wang, G. Yang, Y. Qi, T. Chai, S. Li and T. Zhu, *Sep. Purif. Technol.*, 2018, **202**, 335–344, DOI: 10.1016/j.seppur.2018.04.013.
55 A. Kumar and A. K. Rai, *Int. J. Basic Appl. Sci.*, 2013, **2**, 56–59.
56 Y. Huang, H. Pan, H. Liu, Y. Xi and D. Ren, *Toxicon*, 2019, **169**, 103–108, DOI: 10.1016/j.toxicon.2019.09.004.
57 O. Liran, E. Shemesh and D. Tchernov, *Algal Res.*, 2018, **33**, 419–429, DOI: 10.1016/j.algal.2018.06.020.
58 F. Fang, Y. Gao, L. Gan, X. He and L. Yang, *J. Appl. Phycol.*, 2018, **30**, 1777–1793, DOI: 10.1007/s10811-018-1394-5.
59 J. Yang, H. Tang, X. Zhang, X. Zhu, Y. Huang and Z. Yang, *Environ. Sci. Pollut. Res.*, 2018, **25**, 4794–4802, DOI: 10.1007/s11356-017-0887-0.
60 X. Wang, C. Hao, F. Zhang, C. Feng and Y. Yang, *Bioresour. Technol.*, 2011, **102**, 5742–5748, DOI: 10.1016/j.biortech.2011.03.015.
61 K. Gao, J. Beardall, D.-P. Häder, J. M. Hall-Spencer, G. Gao and D. A. Hutchins, *Front. Mar. Sci.*, 2019, **6**, 322, DOI: 10.3389/fmars.2019.00322.
62 T. Kallas and R. W. Castenholz, *J. Bacteriol.*, 1982, **149**, 237–246, DOI: 10.1128/jb.149.1.237-246.1982.
63 N. Giraldez-Ruiz, P. Mateo, I. Bonilla and F. Fernandez-Piñas., *New Phytol.*, 1997, **137**, 599–605, DOI: 10.1046/j.1469-8137.1997.00864.x.
64 G. S. Sree, S. M. Botsa, B. J. M. Reddy and K. B. Ranjitha, *Arabian J. Chem.*, 2020, **13**, 5137–5150, DOI: 10.1016/j.arabjc.2020.02.012.
65 G. Fan, L. Hong, J. Luo, Y. You, J. Zhang, P. Hua and B. Du, *Chem. Eng. J.*, 2019a, 123767, DOI: 10.1016/j.cej.2019.123767.
66 X. Kong, C. Zeng, X. Wang, J. Huang, C. Li, J. Fei, J. Li and Q Feng, *Sci. Rep.*, 2016, **6**, 29049, DOI: 10.1038/srep29049.
67 S. Wan and S. Dong, *Adv. Mater. Res.*, 2014, **827**, 34–37, DOI: 10.4028/www.scientific.net/AMR.827.34.
68 J. Song, W. Xu, J. Ma, W. Xin, J. Wang and J. Zhao, *Appl. Catal., B*, 2018, **226**, 83–92, DOI: 10.1016/j.apcatb.2017.12.034.
69 C. Xiaojuan, Y. Gao and P. Liu, *Appl. Sci.*, 2018, **8**(11), 2073, DOI: 10.3390/app8112073.
70 Z.-X. Lu, L. Zhou, Z.-L. Zhang, W.-L. Shi, Z.-X. Xie, H.-Y. Xie, D.-W. Pang and P. Shen, *Langmuir*, 2003, **19**, 8765–8768, DOI: 10.1021/la034807r.
71 T. Matsuno, T. Goto, S. Ogami, H. Morimoto, K. Yamazaki, N. Inoue, H. Matsuyama, K. Yoshimune and I. Yumoto, *Front. Microbiol.*, 2018, **9**, 2331, DOI: 10.3389/fmicb.2018.02331.
72 T. C. Summerfield and L. A. Sherman, *Appl. Environ. Microbiol.*, 2008, **74**, 5276–5284, DOI: 10.1128/AEM.00883-08.
73 T. A. McConnaughey and J. F. Whelan, *Earth-Sci. Rev.*, 1997, **42**, 95–117, DOI: 10.1016/S0012-8252(96)00036-0.
74 V. Chaturvedi and P. Verma, *Bioresour. Bioprocess.*, 2015, **2**, 18, DOI: 10.1186/s40643-015-0048-6.
75 R. Bacsa, J. Kiwi, T. Ohno, P. Albers and V. Nadtochenko, *J. Phys. Chem. B.*, 2005, **109**, 5994–6003, DOI: 10.1021/jp044979c.
76 G. Fan, Y. You, B. Wang, S. Wu, Z. Zhang, X. Zheng, M. Bao and J. Zhan, *Appl. Catal., B*, 2019b, **256**, 117866, DOI: 10.1016/j.apcatb.2019.117866.
77 W. Xin, W. Xuejiang, J. Zhao, J. Song and C. Su, *Water Res.*, 2018, **131**, 320–333, DOI: 10.1016/j.watres.2017.12.062.
78 J. R. Peller, R. L. Whitman, S. Griffith, P. Harris, C. Peller and J. Scalzitti, *J. Photochem. Photobiol., A*, 2007, **186**, 212–217, DOI: 10.1016/j.jphotochem.2006.08.009.
79 N. Gu, J. Gao, K. Wang, B. Li, W. Dong and Y. Ma, *J. Taiwan Inst. Chem. Eng.*, 2016, **64**, 189–195, DOI: 10.1016/j.jtice.2016.04.016.
80 C. A. Linkous, G. J. Carter, D. B. Locuson, A. J. Ouellette, D. K. Slattery and L. A. Smitha, *Environ. Sci. Technol.*, 2000, **34**, 4754–4758, DOI: 10.1021/es001080+.
81 W. Xin, W. Xuejiang, J. Zhao, J. Song, J. Wang, R. Ma and J. Ma, *Chem. Eng. J.*, 2017, **320**, 253–263, DOI: 10.1016/j.cej.2017.03.062.
82 X. Yu, J. Zhou, Z. Wang and W. Cai, *J. Photochem. Photobiol., B*, 2010, **101**, 265–270, DOI: 10.1016/j.jphotobiol.2010.07.011.
83 W.-J. Chen, P.-J. Tsai and Y.-C. Chen, *Small*, 2008, **4**, 485–491, DOI: 10.1002/smll.200701164.
84 Y.-H. Tsuang, J.-S. Sun, Y.-C. Huang, C.-H. Lu, W. H.-S. Chang and C.-C. Wang, *Artif. Organs*, 2008, **32**, 167–174, DOI: 10.1111/j.1525-1594.2007.00530.x.
85 S. Natarajan, D. S. Lakshmi, V. Thiagarajan, P. Mrudula, N. Chandrasekaran and A. Mukherjee, *J. Environ. Chem. Eng.*, 2018, **6**, 6870–6880, DOI: 10.1016/j.jece.2018.10.050.
86 H. Baniamerian, P. Tsapekos, M. Alvarado, S. Shokrollahzadeh, M. Safavi and I. Angelidaki, *Chemosphere*, 2019, **242**, 125119, DOI: 10.1016/j.chemosphere.2019.125119.
87 A. F. Halbus and T. S. Horozov, *Nanoscale Adv.*, 2019, **1**, 2323–2336, DOI: 10.1039/c9na00099b.
88 G. Fan, B. Du, J. Zhou, Z. Yan, Y. You and J. Luo, *Chem. Eng. J.*, 2021a, **404**, 126509, DOI: 10.1016/j.cej.2020.126509.
89 G. Fan, J. Zhan, J. Luo, J. Lin, F. Qu, B. Du, Y. You and Z. Yan, *J. Hazard. Mater.*, 2021b, **404**, 124062, DOI: 10.1016/j.jhazmat.2020.124062.
90 G. Fan, C. Cai, Z. Chen, J. Luo, B. Du, S. Yang and J. Wu, *J. Hazard. Mater.*, 2023, **441**, 129932, DOI: 10.1016/j.jhazmat.2022.129932.